Quantifying Structure and Dynamics of the Open-Field Solar Corona

Vadim Uritsky[1,2], Shaela Jones-Mecholsky [1,2], Christopher Rura [1,2], Nick Arge [1], and Nathalia Alzate [1,3]

(1) NASA / Goddard Space Flight Center, Greenbelt, MD
(2) Catholic University of America, Washington, DC
(3) ADNET Systems, Lanham, MD

Summary

Open-field regions of the solar corona play instrumental role in producing the ambient solar wind outflow. Accuracy of the existing space weather prediction models is limited by our ability to measure open magnetic flux in the polar regions, and to establish realistic inner boundary conditions beyond the potential-field extrapolation of the photospheric magnetograms. The structure of the open field corona is coupled to its transient dynamics in the form of field-aligned plasma flows, magnetosonic waves, propagating discontinuities, etc.

We present two groups of image analysis methods providing new insights into the spatiotemporal evolution of the open corona.

1) The Quasi-Radial Field-line Tracing (QRaFT) method and code package enable an identification of the field-line geometry based on high-resolution coronagraph observations. QRaFT detects and segments large-scale azimuthal gradients in the polarized brightness signal and computes their plane-of-sky orientation angles which approximate the magnetic field orientation. We show examples of QRaFT-based processing of STEREO COR1 and MLSO K-Cor images and discuss how these results can be used to optimize global coronal and heliospheric models such as WSA/ADAPT/ENLIL.

2) The surfing transform (ST) technique is a sensitive tool for measuring transient propagating disturbances in the open-field corona. ST-based tracking enables robust evaluation of local plasma velocity and acceleration across a wide range of radial distances, and can be efficiently used to quantify the kinematics of both small- and large-scale propagating disturbances constrained by the expanding quasi-radial field.

We argue that a simultaneous application of the two groups of methods can provide important new information about the physical coupling between the geometry and the dynamics of the open-flux solar corona imaged by the upcoming PUNCH mission.

Quasi-Radial Field-line Tracing (QRaFT) Software for Constraining Global Coronal and Heliospheric Models

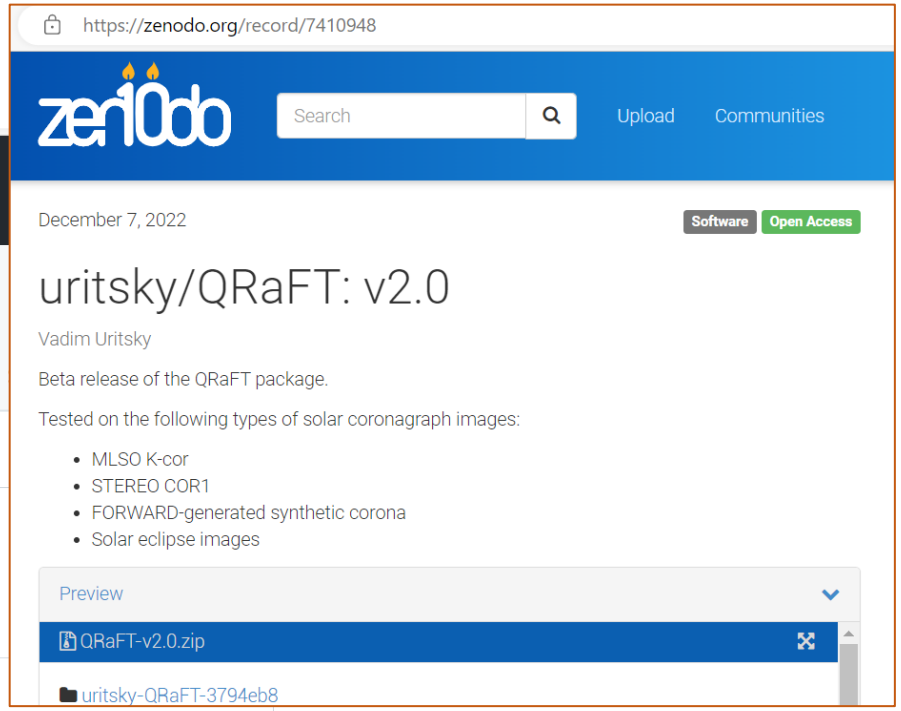

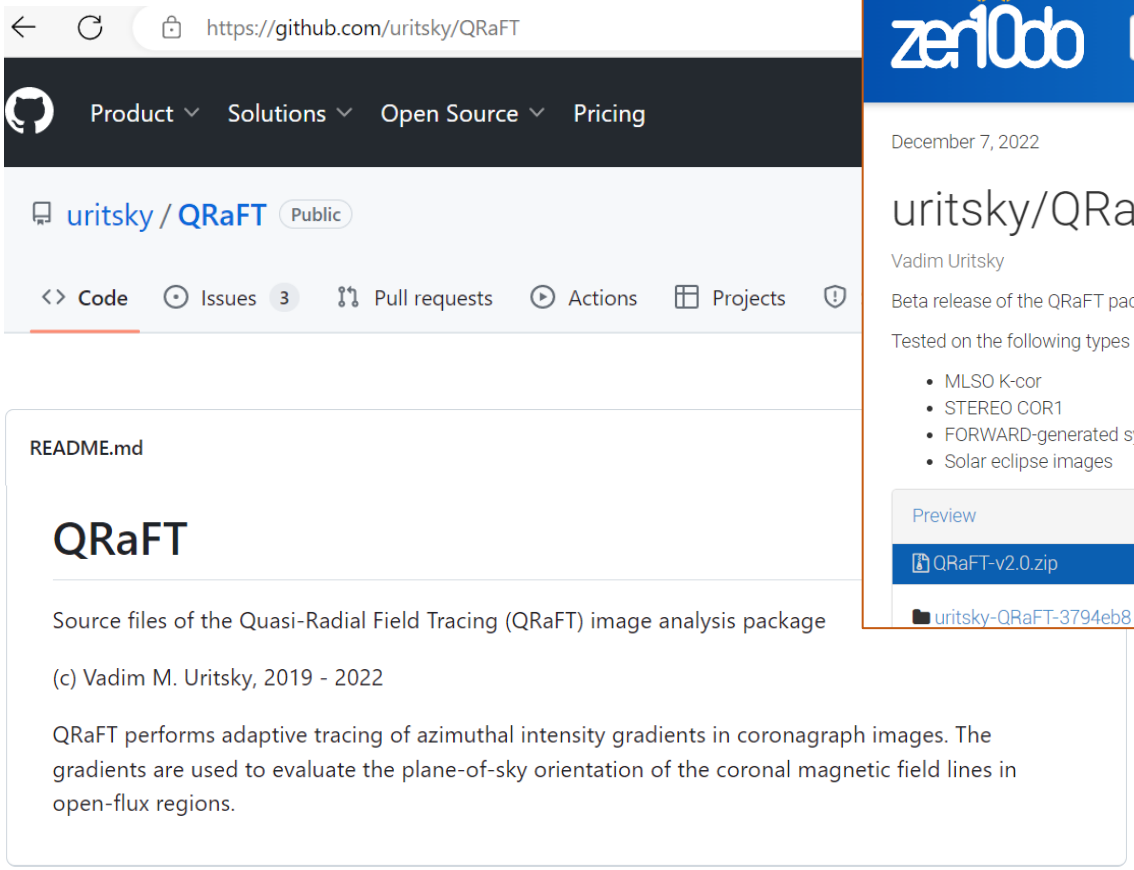

V. Uritsky. Quasi-Radial Field-line Tracing (QRaFT v2.0): an image analysis package for reconstructing the magnetic field geometry of the open-flux solar corona, *GitHub / Zenode*, 2022, URL: github.com/uritsky/QRaFT, DOI:10.5281/zenodo.7410948

Magnetic alignment of quasi-radial density structures

$$\rho\left(\frac{\partial\vec{v}}{\partial t}+\vec{v}\cdot\nabla\vec{v}\right)=-\nabla p+\vec{j}\times\vec{B}+\rho\,\vec{g_S}$$

Simplifying assumptions

(1) The plasma flow is laminar and constrained by a quasi-radial $\vec{B}$ field, so that $\nabla\times\vec{v}\perp\vec{B}$ and the convective derivative on the left hand side of (3) is reduced to $\nabla_{\|}v^2/2$.
(2) The plasma consists of entirely ionized hydrogen and helium atoms so that the mass density $\rho=(f_H+4f_{He})nm_p\equiv\gamma nm_p$, where f_H and f_{He} are fractional abundances by number ($f_H+f_{He}\approx 1$) of respectively hydrogen and helium, n is the proton number density, and m_p is the proton mass. In the following analysis, we use the nominal He/H abundance ratio of 0.06 (Schmelz et al., ApJ 2012) yielding $\gamma\approx 1.2$.
(3) The relationship between the pressure, number density and the temperature T of the plasma is reasonably represented by the ideal gas law $p=2nk_BT$, in which k_B is the Boltzmann constant,
(4) The plasma is isothermal along the magnetic field ($\nabla_{\|}T=0$).

$$\cos\beta\approx\frac{\ell_n(r)\gamma m_p\cos\alpha}{2k_BT}\left[\frac{d}{dr}\left(\frac{v_{PSW}^2(r,T)}{2}\right)+g_S(r)\right];\quad\theta=90^\circ-\beta$$

$$\ell_n=\frac{n}{|\nabla n|}$$

$$\cos\beta \approx \frac{\ell_n(r)\gamma m_p \cos\alpha}{2k_B T}\left[\frac{d}{dr}\left(\frac{v_{PSW}^2(r,T)}{2}\right) + g_S(r)\right];\ \ \theta = 90^\circ - \beta$$

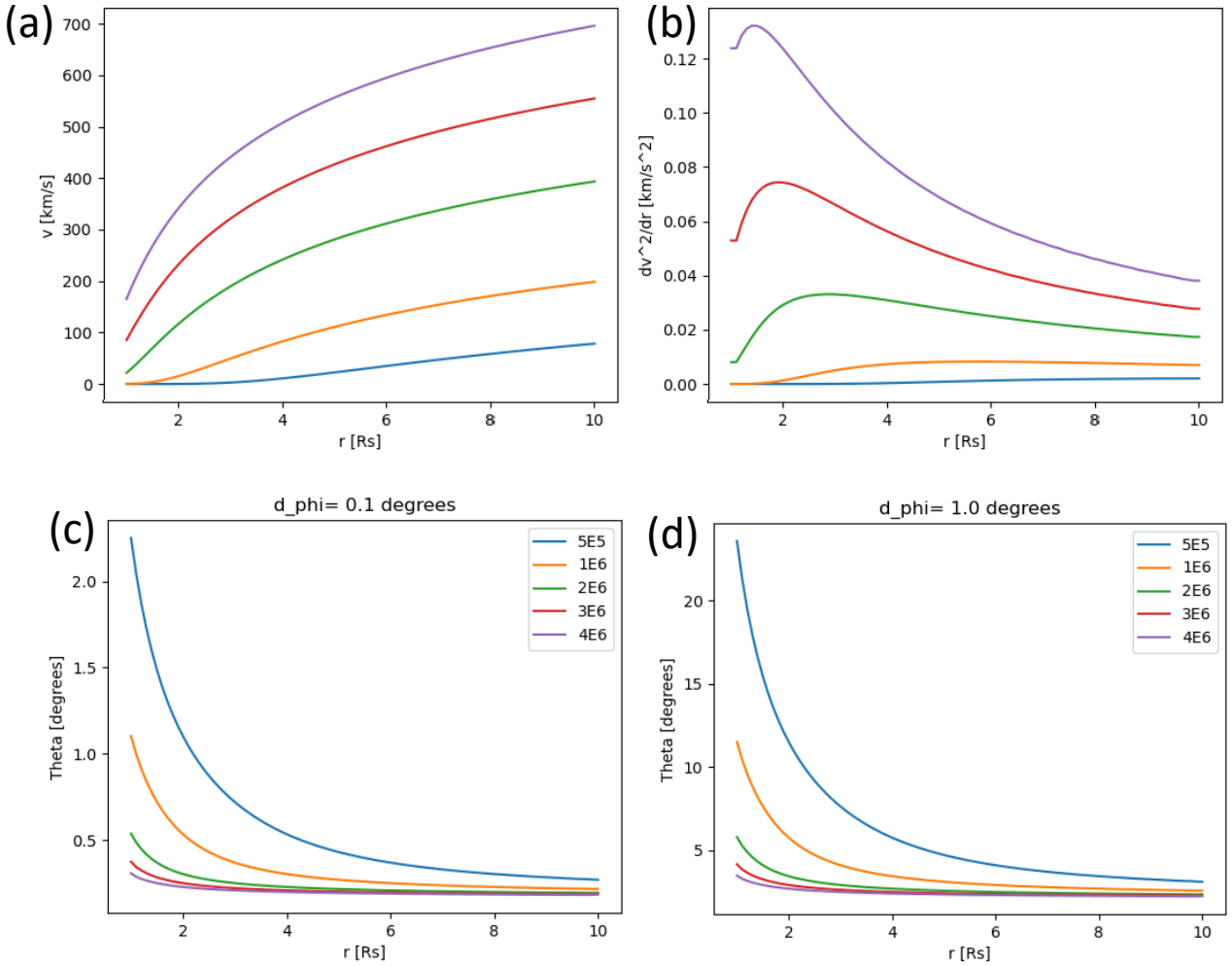

Segmenting a K-Cor MLSO image by QRaFT

2016/05/27 16:55:33

Original Level 1 K-Cor image

Unsigned 1st-Order Azimuthal Detrended Difference

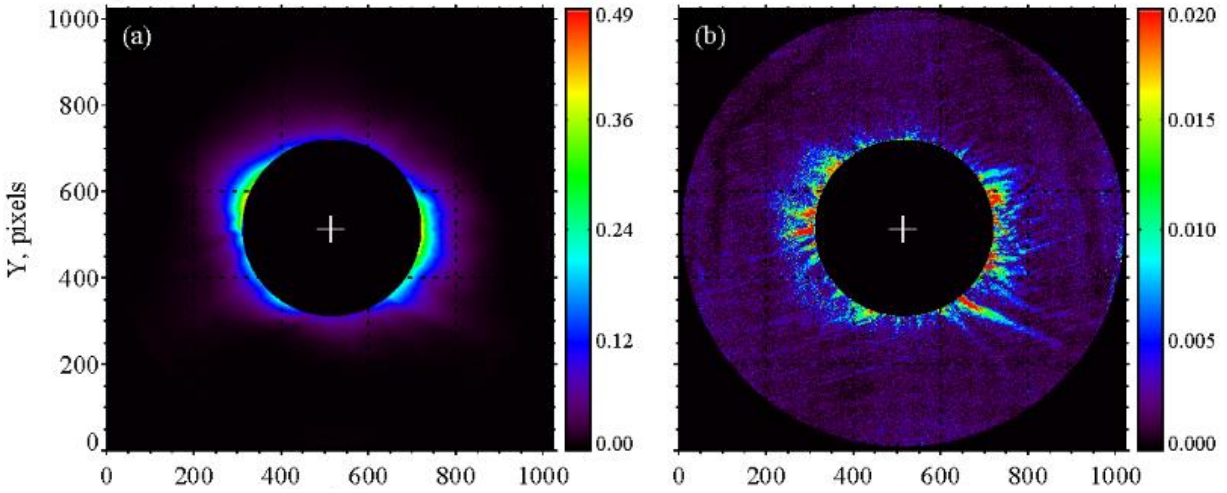

2nd-Order Difference in Polar Coordinates

Features Detected

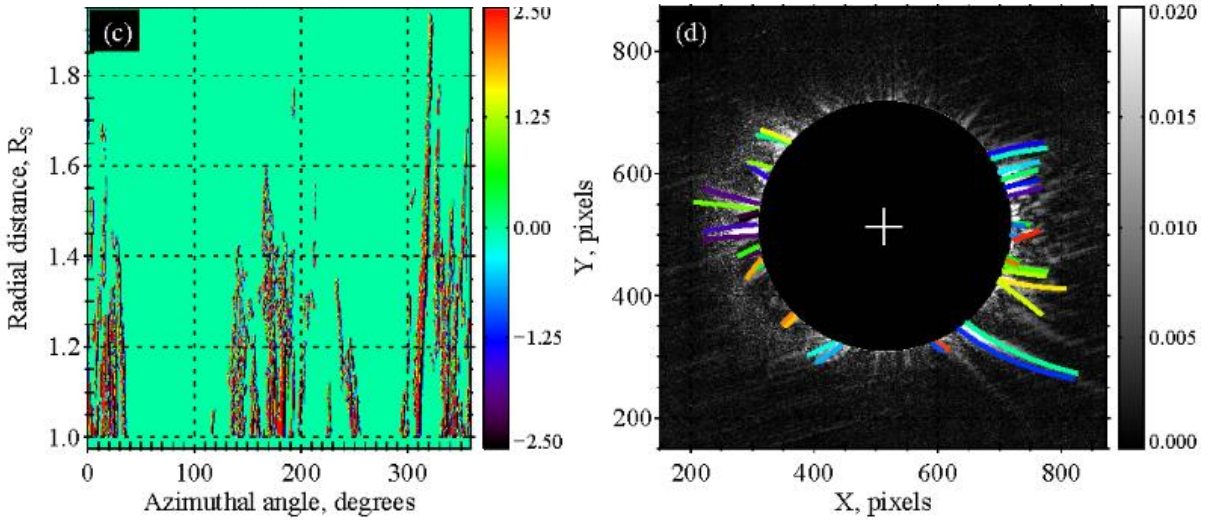

Uritsky pub. in prep. 2023

Testing QRaFT Performance on a Simulated Corona
(Predictive Science Inc MAS model + FORWARD code)

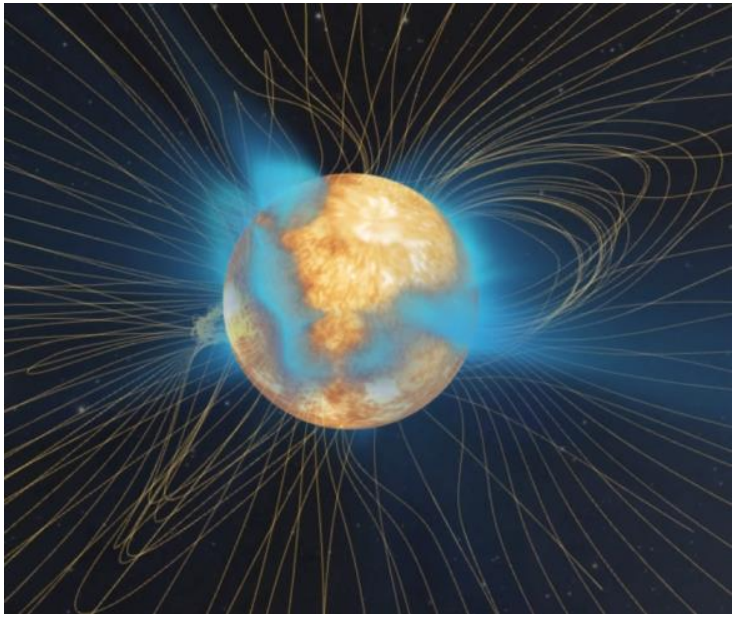

Aug-Sep 2017, CR 2194

Z. Mikic, C. Downs, J. Linker et al., Predicting the corona for the 21 August 2017 total solar eclipse, Nature Astronomy 2018

S. Gibson, T. Kucera, S. White et al., FORWARD: A Toolset for Multiwavelength Coronal Magnetometry, Front. Astron. Space Sci 2016.

Validating QRaFT Performace

PSI MAS magnetic field

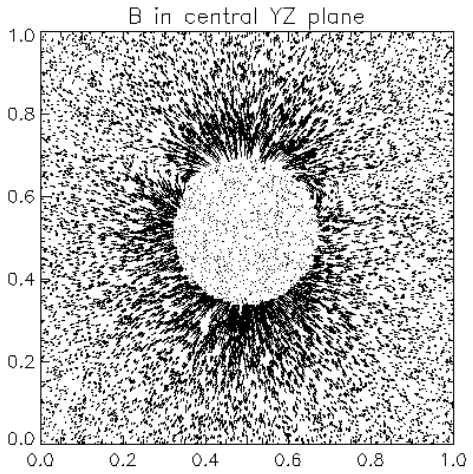

FORWARD pB image

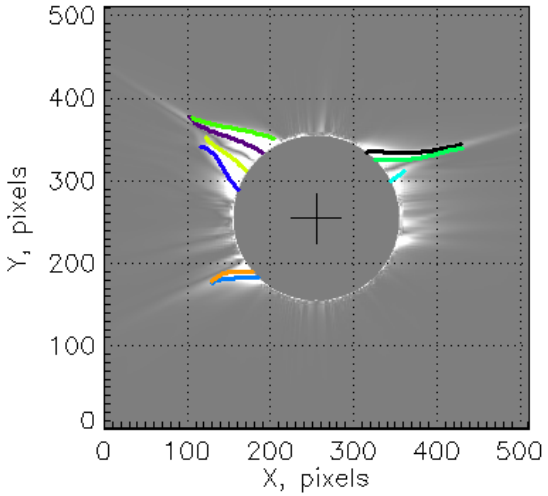

Coaligned STEREO COR1 image

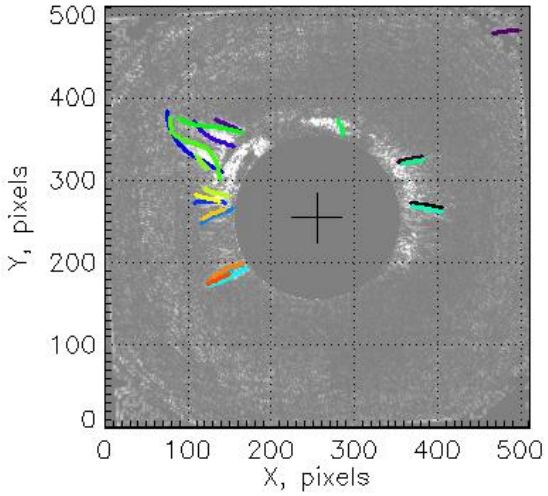

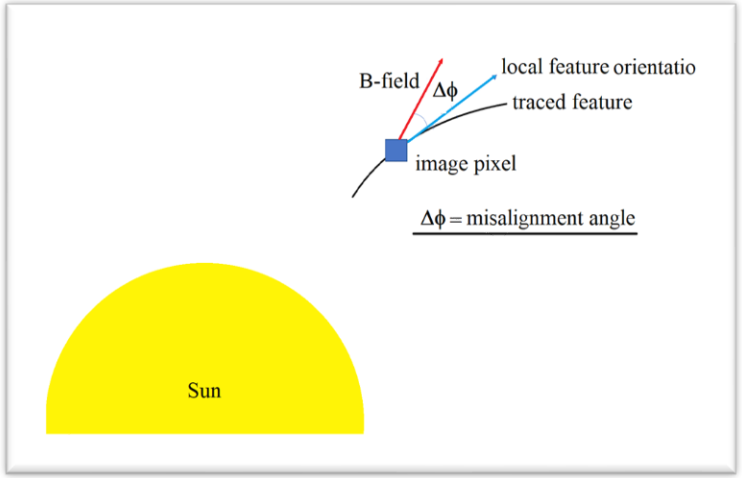

Statistical Analysis of Tracing Errors

PSI MAS magnetic field

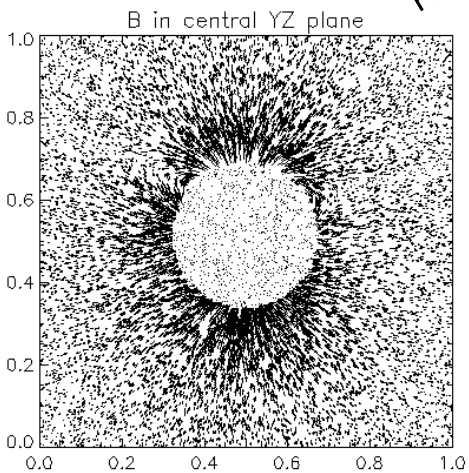

FORWARD vs PSI

COR1 vs PSI

FORWARD pB image

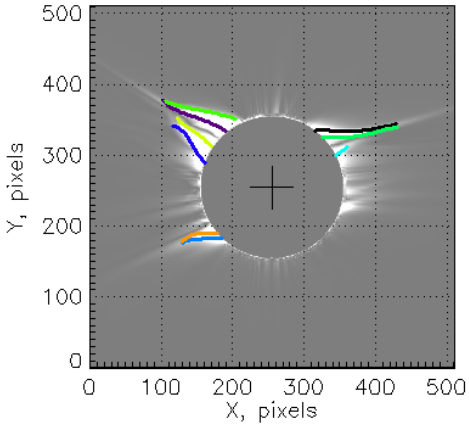

STEREO COR1 image

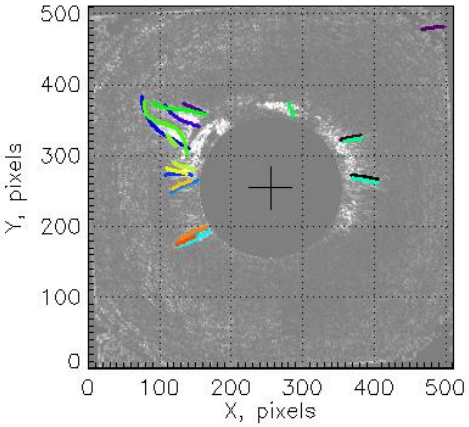

Statistics of discrepancy errors

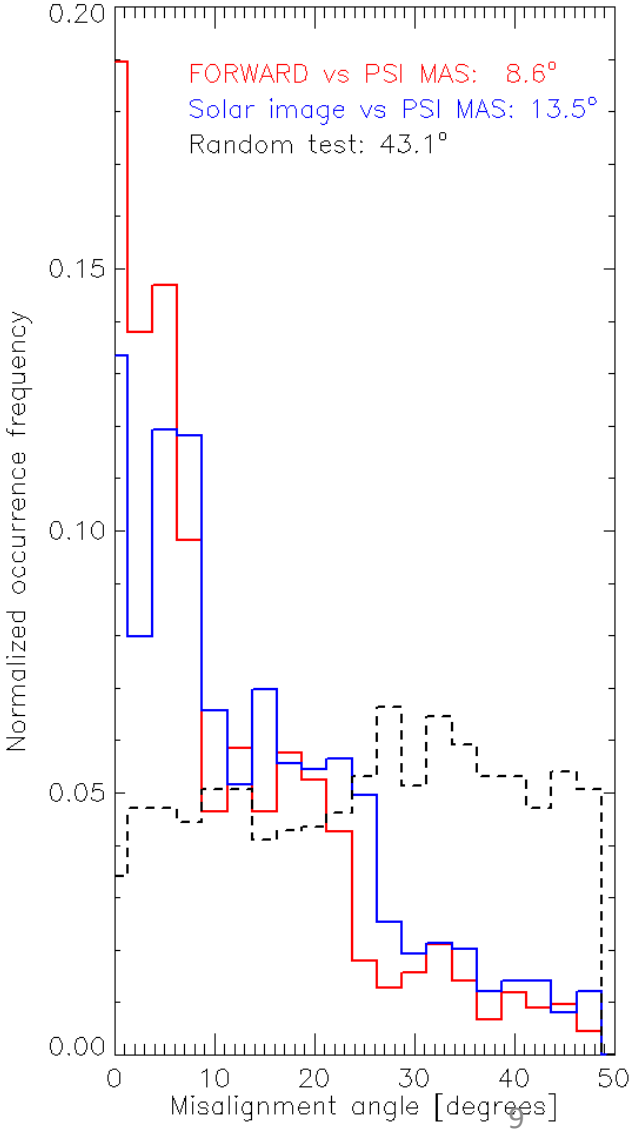

Framework to Validate QRaFT Segmentation

(C. Rura et al.., in prep.)

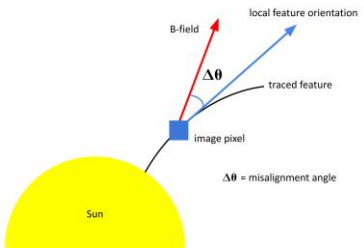

Image Based Framework for Assessing Coronal Magnetic Field Models

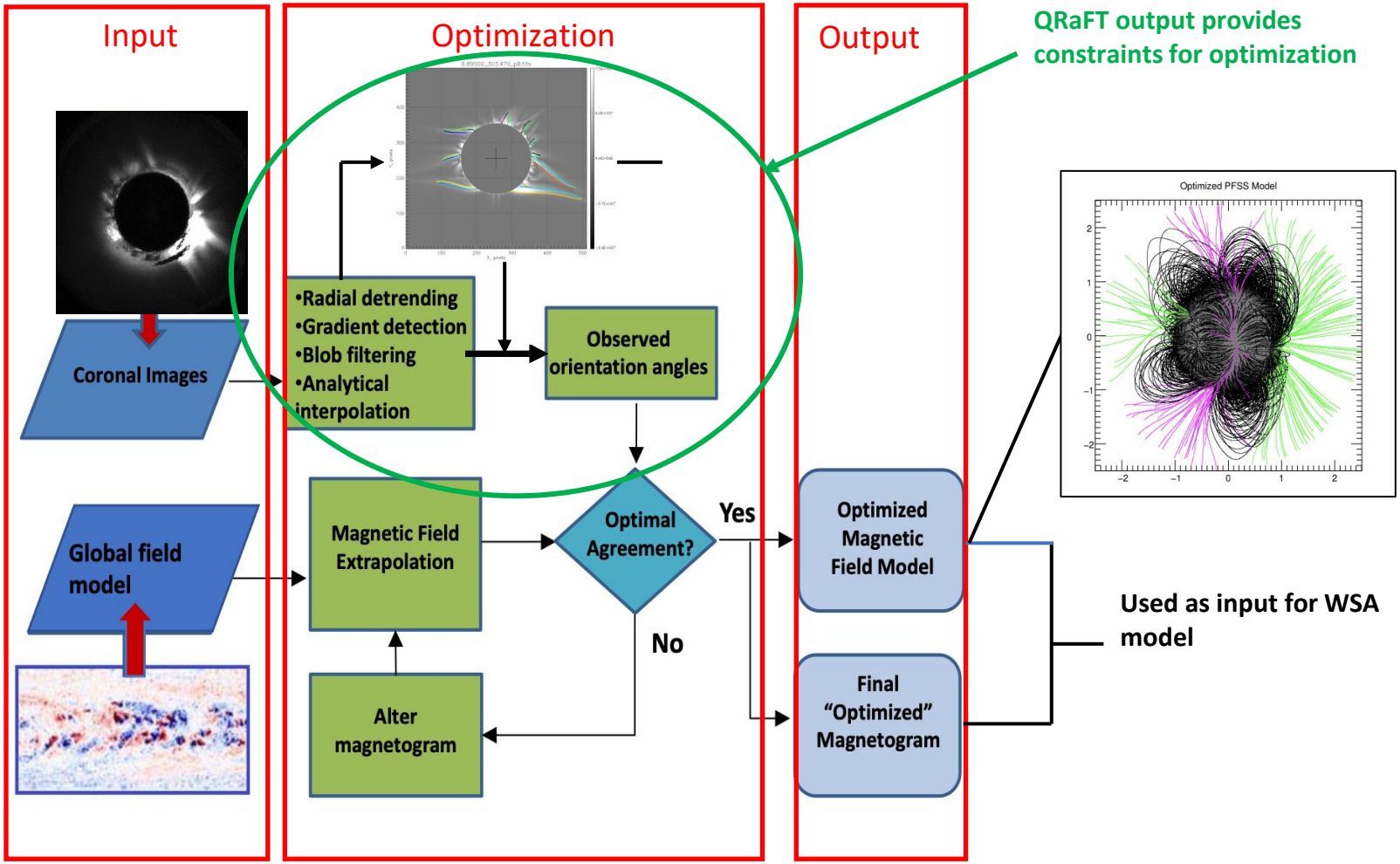

QRaFT validation results

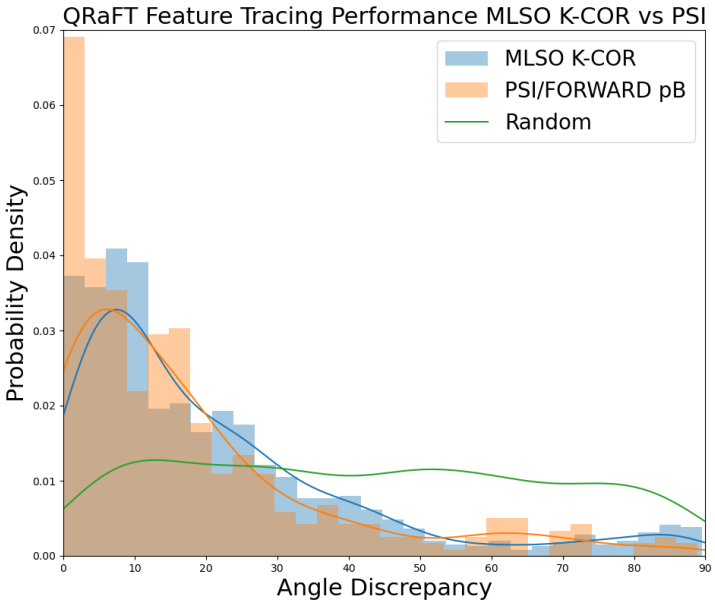

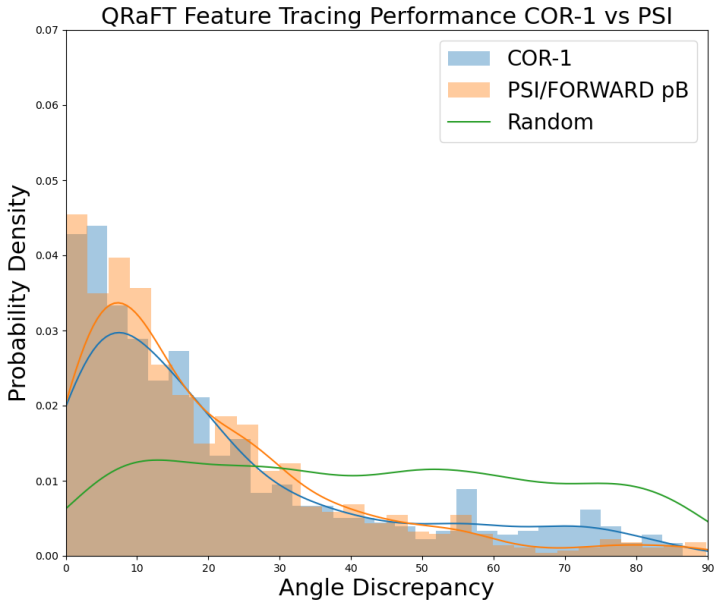

Table 1. Average and Median Angle Discrepancies of Orientation of Traced Features when Compared to Model Magnetic Field Orientation

Statistical Metric	Average Discrepancy	Median Discrepancy
PSI/FORWARD	17.645°	12.189°
MLSO K-COR	20.916°	14.110°
STEREO COR-1	21.594°	14.497°
Random	42.242°	41.147°

Comparing ADAPT-WSA Corona B Field Solutions with Observations

MLSO MK4 White Light

QRaFT

ADAPT-WSA Coronal Field

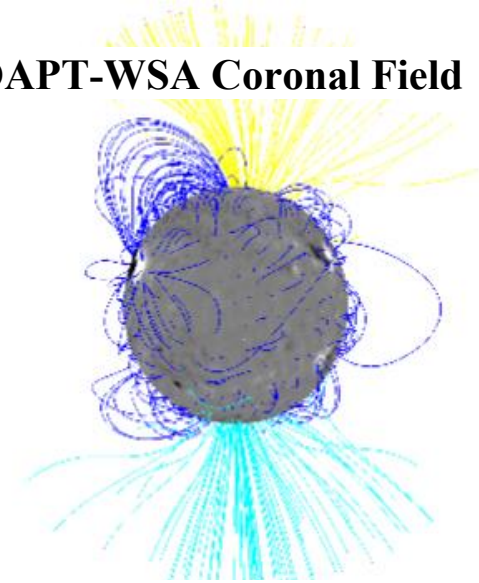

Discrepancy between orientation of features seen in images $\{\theta_o\}$ and magnetic field model $\{\theta_m\}$:

$$J = \beta \sum_{k=1}^{N} |\theta_{o,k} - \theta_{m,k}|^d$$

- Assumes obs. features lie in the image plane
- Assumes constraints are equally valid
- Decreases with better model quality

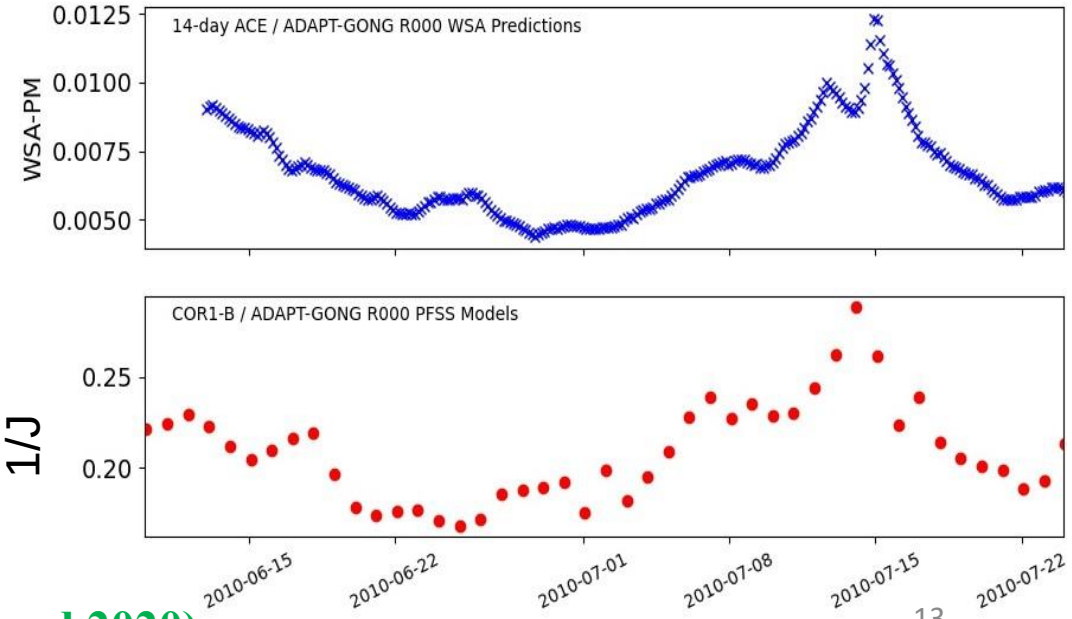

For more details see Jones et al. (2017 and 2020)

Measuring Outflow Velocity Using the Surfing Transform (ST) Technique

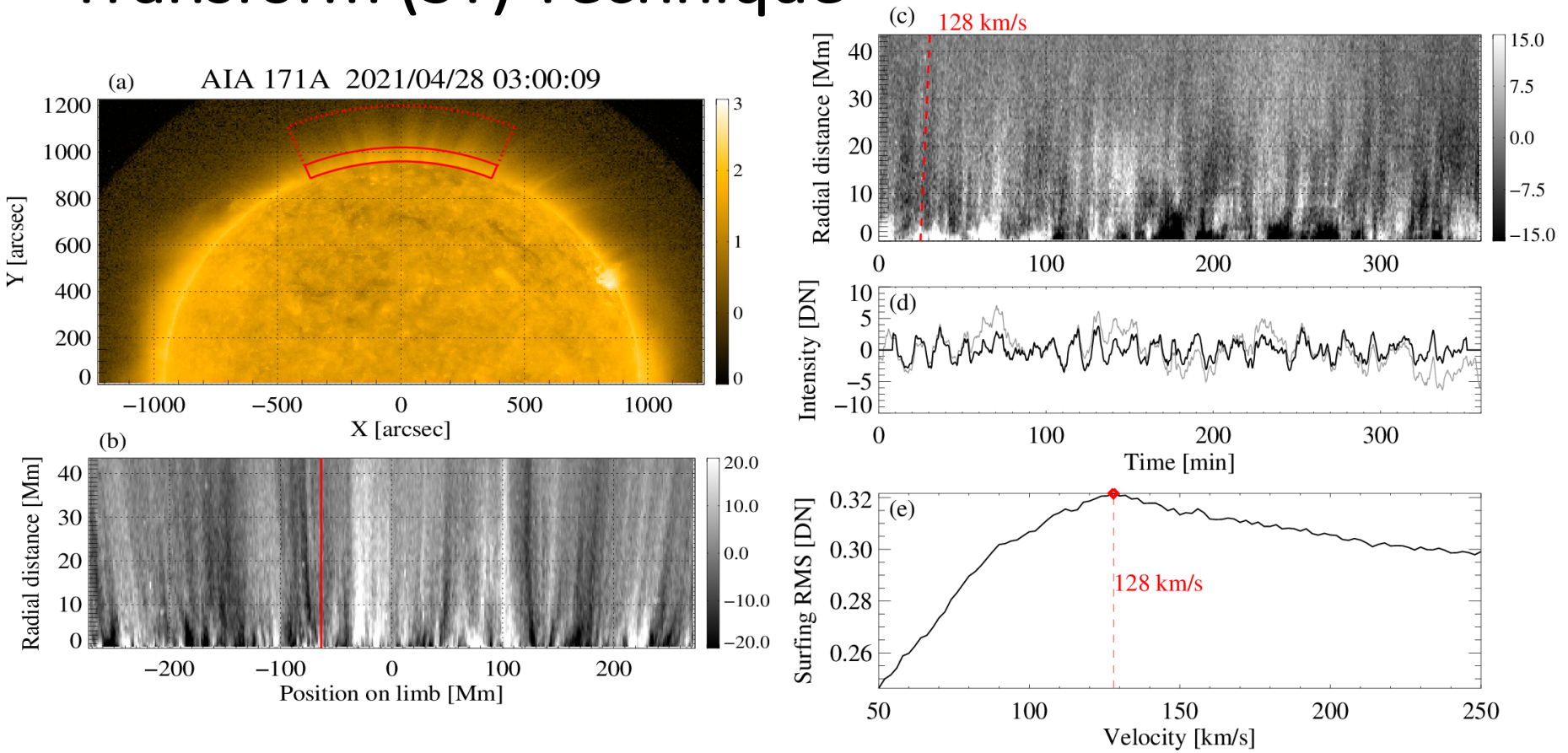

(a) One of 1,800 processed SDO AIA 171A images, with the regions of interest bounded by the red lines. (b) Polar coordinate representation of the main ROI of the SDO AIA image on panel (a). (c) A time-distance plot representing time evolution of the lower corona along the radial slit marked with a green dashed line on the panel (b). A spatio-temporal direction corresponding to the propagation velocity measured by the surfing analysis method is shown with a red dashed line. (d) The maximized surfing signal S(t, u = v) fulfilling the resonance condition, before and after temporal detrending (grey and black lines, correspondingly). (e) The RMS value of the surfing signal S(t, u) for the time-distance plot in panel (c), showing a resonance behavior at $u = v$ **(Uritsky et al., 2013, 2022, 2023 [in prep.])**

Estimated Outflow Speed along the Limb

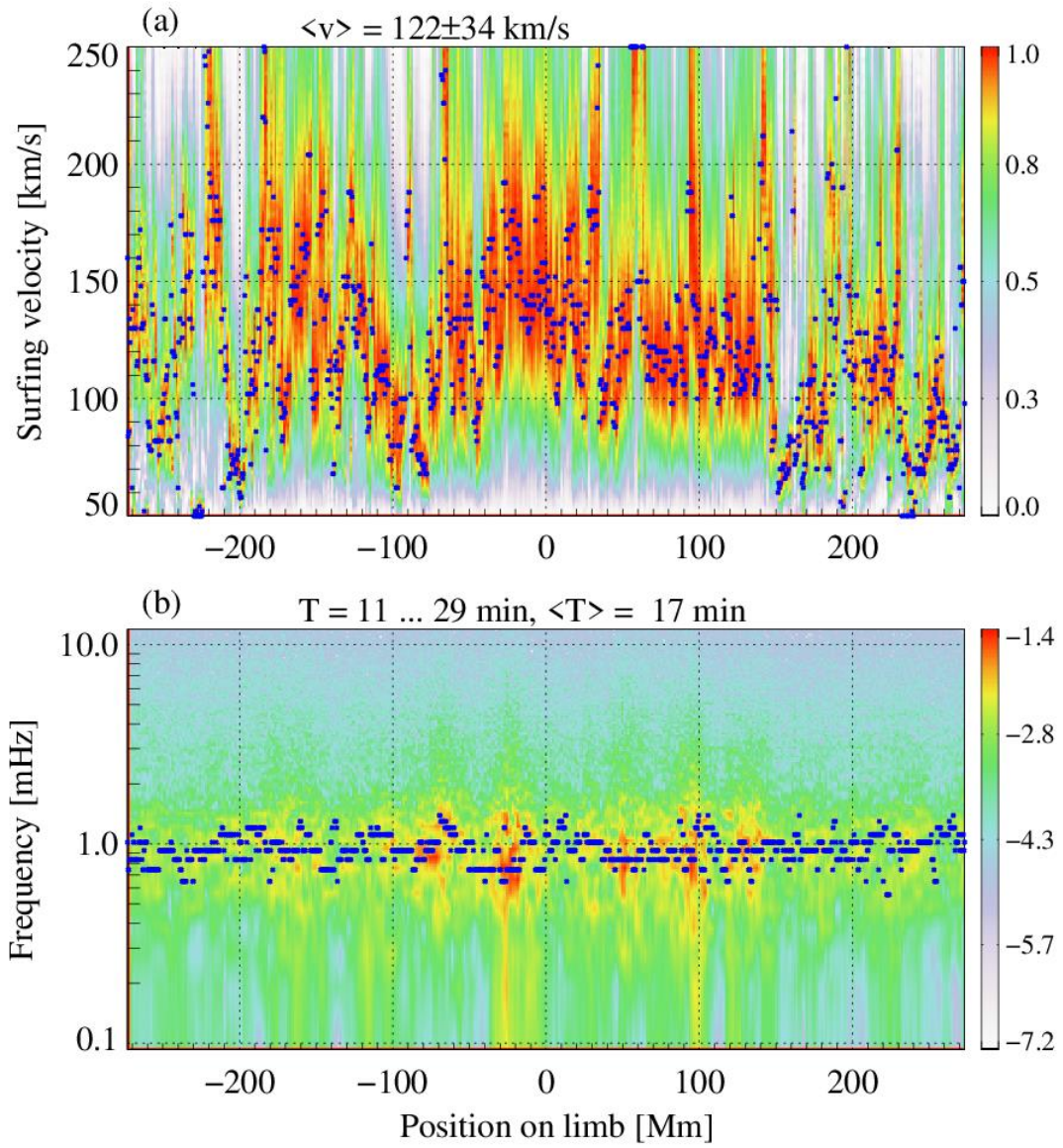

ST analysis of the coronal outflow velocity. (a) Velocity dependence of the surfing RMS for each location on the limb. Each vertical slice represents a dependence of the surfing RMS on the attempted surfing velocity, with the blue dot showing the position of the resonance maximum used to identify the propagation speed. (b) Fourier power spectra of the resonance surfing signals for different limb positions. The blue dots show the spectral peaks used to evaluate the dominating frequency. Temporal trends longer than 20 min were removed for a more accurate velocity estimation.

Spatiotemporal Map of Transient Flows

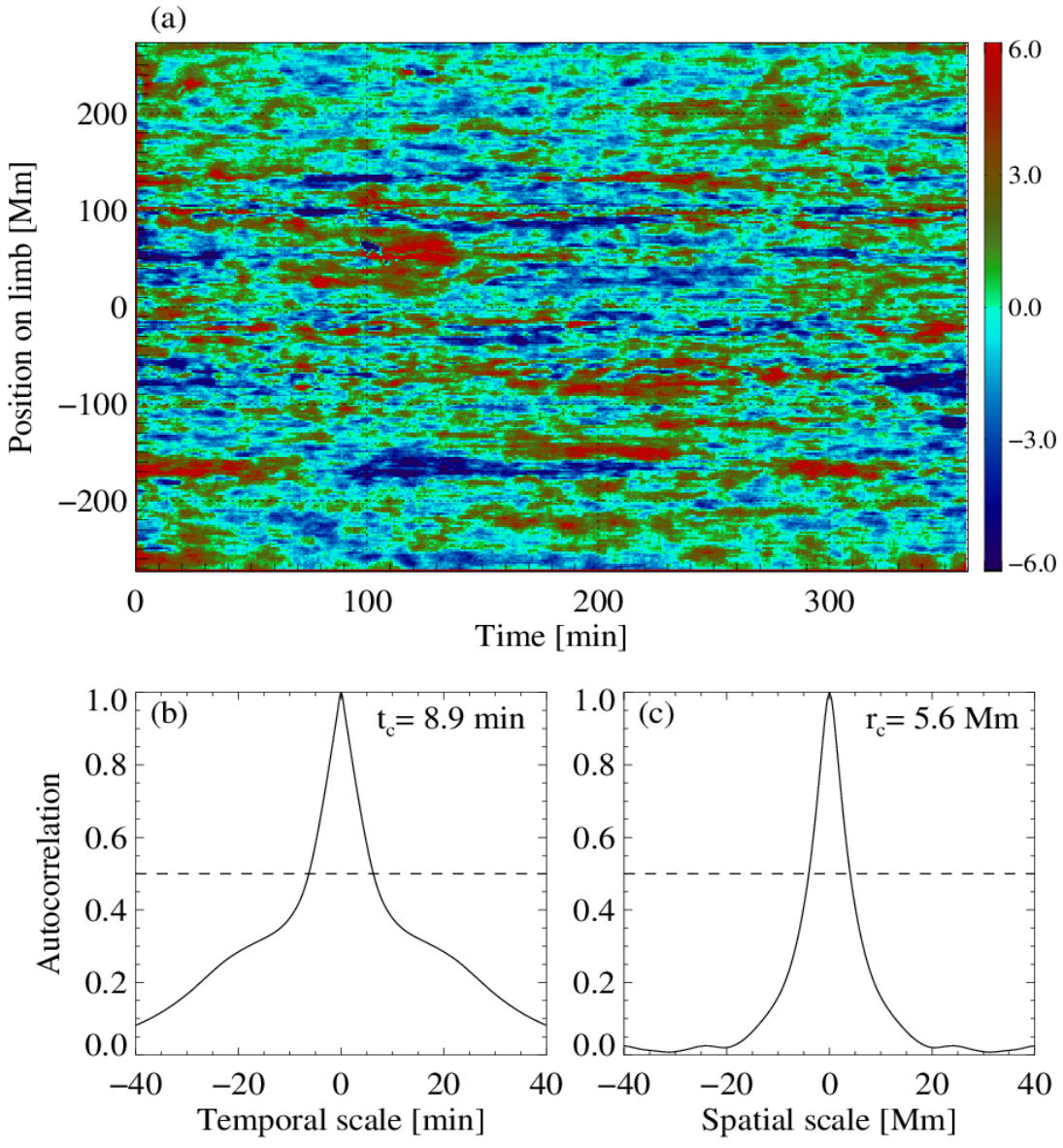

(a) Spatiotemporal map of the transient outflow in the studied region constructed using the ST technique. The compact blobs shown in red represent starting times and locations of the quasi-periodic propagating fronts. (b,c) Temporal and spatial autocorrelation functions of the surfing signals; the estimated characteristic scales represent the 50% levels and assume an exponential decay.

Statistics of Outflow Parameters
(based on ~2,500 events)

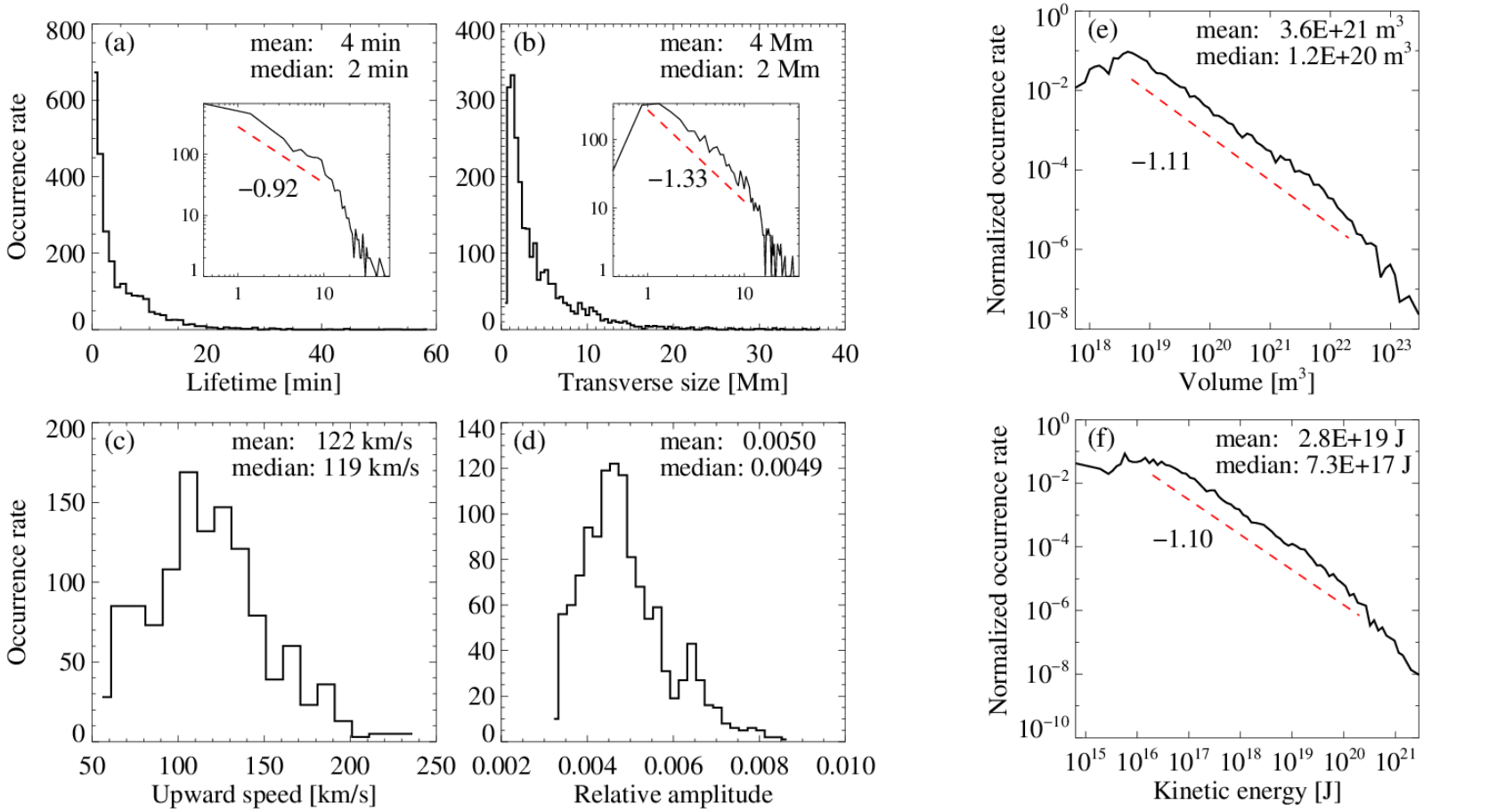

Probability histograms of the detected transient flow events over (a) the event lifetime, (b) flow transverse size, (c) upward flow velocity, (d) relative emission intensity, (e) flow volume, and (f) flow kinetic energy. Mean and median values of each parameter are provided. The dashed red lines show the log-log slopes of the distributions, supplemented by the evaluated power-law exponents.

References

- C. Rura, V. Uritsky, S. Jones, N. Arge, and N. Alzate, Validation of Image Based Method for Assessing Coronal Magnetic Field Models, 2023 [in prep.]
- S. Jones, T. Wang, N. Arge et al., Quantitative Evaluation of Coronal Magnetic Field Models Using Tomographic Reconstructions of Electron Density, APJ 2022
- S. Jones, V. Uritsky, J. Davila, and V. Troyan, Improving Coronal Magnetic Field Models Using Image Optimization, ApJ 2020.
- S. Jones, V. Uritsky, and J. Davila, Image-optimized Coronal Magnetic Field Models, ApJ 2017.
- S. Jones, V. Uritsky, and J. Davila, Optimizing Global Coronal Magnetic Field Models Using Image-based Constraints, ApJ 2016.
- V. Uritsky. Quasi-Radial Field-line Tracing (QRaFT v2.0): an image analysis package for reconstructing the magnetic field geometry of the open-flux solar corona, GitHub / Zenode, 2022, URL: github.com/uritsky/QRaFT, DOI:10.5281/zenodo.7410948
- V. Uritsky et al., Statistical survey of multiscale transients at the source of the fast solar wind, ApJL, 2023 [in prep.]
- V. Uritsky, C. DeForest, J. Karpen et al., Plumelets: Dynamic Filamentary Structures in Solar Coronal Plumes, ApJ 2021.
- V. Uritsky, J. Davila, N. Viall, and L. Ofman. Measuring Temperature-dependent Propagating Disturbances in Coronal Fan Loops Using Multiple SDO/AIA Channels and the Surfing Transform Technique, ApJ 2013.